Eur. Phys. J. B **45**, 237–242 (2005)
DOI: 10.1140/epjb/e2005-00181-8

THE EUROPEAN PHYSICAL JOURNAL B

Structural and magnetic properties of ion-beam deposited NiFe/Co-oxide bilayers

K.-W. Lin[a], F.-T. Lin, Y.-M Tzeng, and Z.-Y. Guo

Department of Materials Engineering, National Chung Hsing University, Taichung 402, Taiwan, R.O.C.

Received 15 September 2004 / Received in final form 18 May 2005
Published online 28 June 2005 –

Abstract. The structural and magnetic properties of NiFe/Co-oxide bilayers were studied. XRD investigation indicates the NiFe (Permalloy) layers (a = 3.53 Å) grow with a (111) preferred orientation. The Co-oxide layers were fabricated with oxygen content in the deposition assist beam ranging from 8% (rock-salt CoO, a = 4.27 Å) to 34% (spinel Co_3O_4, a = 8.21 Å). Both the coercivity H_c and exchange bias field H_{ex} closely follow an inverse NiFe thickness relationship. A strong temperature dependence of H_c and H_{ex} is found in these NiFe/Co-oxide bilayers. At T = 289 K, the NiFe/CoO film exhibits an enhanced H_c relative to pure NiFe/Co or NiFe/Co_3O_4 bilayers, an indication of exchange coupling between the NiFe and CoO phases. At T = 10 K, the NiFe/Co_3O_4 film exhibits an exchange-bias loop shift of $H_{ex} \sim -200$ Oe that persists to temperatures greater than 30 K (the Néel temperature of bulk Co_3O_4). The transition temperature of the Co_3O_4 film component has increased above the bulk value via exchange coupling with the permalloy. Results indicate that the exchange coupling interaction between FM and AFM layers are responsible for both enhanced coercivity and cross-tie domains.

PACS. 75.70.Cn Magnetic properties of interfaces (multilayers, superlattices, heterostructures)

1 Introduction

Exchange coupling between a ferromagnet (FM) and an antiferromagnet (AFM) may be understood by the interfacial interaction between FM and AFM moments [1,2]. It is typically characterized by an enhanced coercivity and a field shift in the hysteresis loop, a phenomenon known as exchange coupling. A variety of AFM/FM systems [3,4] have been studied and several theories [5,6] have been proposed to describe the physical properties. Despite technological applications such as magnetic sensors and magnetoresistive random access memory (MRAM), the fundamental mechanisms responsible for exchange bias remain unclear. One difficulty in analyzing the exchange bias effect is the determination of structure and morphology at the interface, which strongly depends on the preparation methods such as metal evaporation/oxidation or sputter deposition [7–9]. In addition, the defects at the interface may be influenced by both the roughness of the substrate and growth conditions [10].

Nanometer-sized cobalt oxide films have drawn much attention in recent decades due to potential applications in spin-valve structures and magnetic random access memory (MRAM) when coupled to a ferromagnetic material (FM) [11–15]. Therefore, many studies have focused on the cobalt-oxygen interaction process. The CoO phase is known to be the major product in the temperature range of 300 K to 500 K, although how the CoO, Co_3O_4 or mixtures of both phases form remains unclear [16,17]. It is known that antiferromagnetic (AF) domain formation plays an important role in exchange coupled systems [18,19]. The energy stored in AF domain walls gives rise to the exchange bias which is proportional to $4(A_{AF}K_{AF})^{1/2}$ [20], where A_{AF} and K_{AF} are the exchange stiffness and anisotropy constant of the AF layer, respectively. The existence of AF domains, necessary for appearance of exchange bias, is usually observed through FM domains coupled to the AF material [21] since direct observation of AF domains is difficult. The aim of this work was to study the effect on exchange bias that arises from different oxide phases of the same parent compound, and the variation in domain wall formation. We do this by examining NiFe layers that are exchange coupled with different forms of Co-oxide layers deposited with a dual ion-beam deposition technique.

2 Experimental method

The Co-oxide layers are deposited with oxygen content in the deposition assist beam ranging from 0% O_2 to 34% O_2 at a rate of 0.3 Å/s onto Si (100) substrates, while the NiFe overlayers are deposited from a commercial $Ni_{80}Fe_{20}$ (known as Permalloy) target at a rate of ∼0.4 Å/s. The

[a] e-mail: kwlin@dragon.nchu.edu.tw

substrates (which are chemically cleaned prior to loading into the chamber) are heated to 100 °C for 1 h immediately prior to deposition. The base pressure of the system is in the low 10^{-7} Torr range, while the pressure during deposition is below 5×10^{-4} Torr. The detailed procedure of film deposition is described elsewhere [22]. The thicknesses for NiFe and Co-oxide layers are 21 nm and 17 nm, respectively. No external magnetic field was applied during deposition. A MAC Science (MXP18) analytical X- ray system (operated at 40 kV, 150 mA, with Cu Kα radiation) was used for X-ray diffraction (XRD) analysis of the crystal structure. A JEOL (JEM-2010) transmission electron microscope (TEM) operating at 200 kV was used for microstructural analysis. In-plane and perpendicular hysteresis loops of the NiFe/Co-oxide bilayers were measured (150 K–300 K) with a commercial vibrating sample magnetometer (VSM). Low-temperature magnetic properties were characterized with a commercial superconducting quantum interference device (SQUID) magnetometer using a maximum applied field of ±2 T. The hysteresis loops were measured parallel to the film surface after being field-cooled (FC) down to 10 K in a 20 kOe. The surface topography and magnetic structures of NiFe/Co-oxide bilayers were investigated by a VEECO (DI-3100) atomic/magnetic force microscope (AFM/MFM). The magnetic domain patterns were obtained at zero field by MFM imaging with the Co-alloy coated tip.

3 Results and discussion

The composition of the NiFe layer is about 79 at. % Ni, 18 at. % Fe, and 3 at. % oxygen, as determined by XPS depth profile analysis [23]. The small amount of oxygen is attributed to background impurities picked up from the (O-ring sealed) chamber wall. Precleaning the target and substrate and then pumping down the chamber to a lower base pressure would help to reduce this impurity effect.

To clarify the relation between composition and exchange coupling in NiFe/Co-oxide bilayers, structural and phase characterization have been carried out with XRD. The grazing-angle XRD patterns of NiFe and CoO are displayed in Figure 1. The ferromagnetic (FM) layer for films prepared with 0% O_2 in the assist beam ($a = 3.53$ Å) grow with a (111) preferred orientation, as shown in Figure 1a. On the other hand, the oxide layer for films prepared with 8% O_2 in the assist beam (Fig. 1b) consists of rock-salt CoO phase ($a = 4.27$ Å) whereas a spinel structure of Co_3O_4 phase ($a = 8.21$ Å) was found for films prepared with 34% O_2 in the assist beam, as shown in Figure 1c.

TEM was used to measure the grain size and verify the crystal structures of these films. Results are shown in Figure 2. The microstructure consisted of fine equiaxed grains of $Ni_{80}Fe_{20}$ (Fig. 2a) that appear to extend throughout the films thickness. Figures 2b, d, and f correspond to the selected diffraction patterns of the $Ni_{80}Fe_{20}$, CoO, and Co_3O_4 layers, in agreement with the X-ray diffraction measurements. For films prepared with 34% O_2 in the assist beam, the oxide structure changed from CoO to spinel Co_3O_4 and the microstructure is clearly observed in Figure 2e. Additionally, films prepared with between 15% and 30% O_2 in the assist beam consisted of a mixture of CoO and Co_3O_4 phases. It should be noted that films prepared with either 8% or 34% O_2 in the assist beam during the Co-oxide deposition had a pure, single oxide phase. That is, either a pure CoO (8% O_2) phase or pure Co_3O_4(34% O_2) phase was deposited. This can clearly be

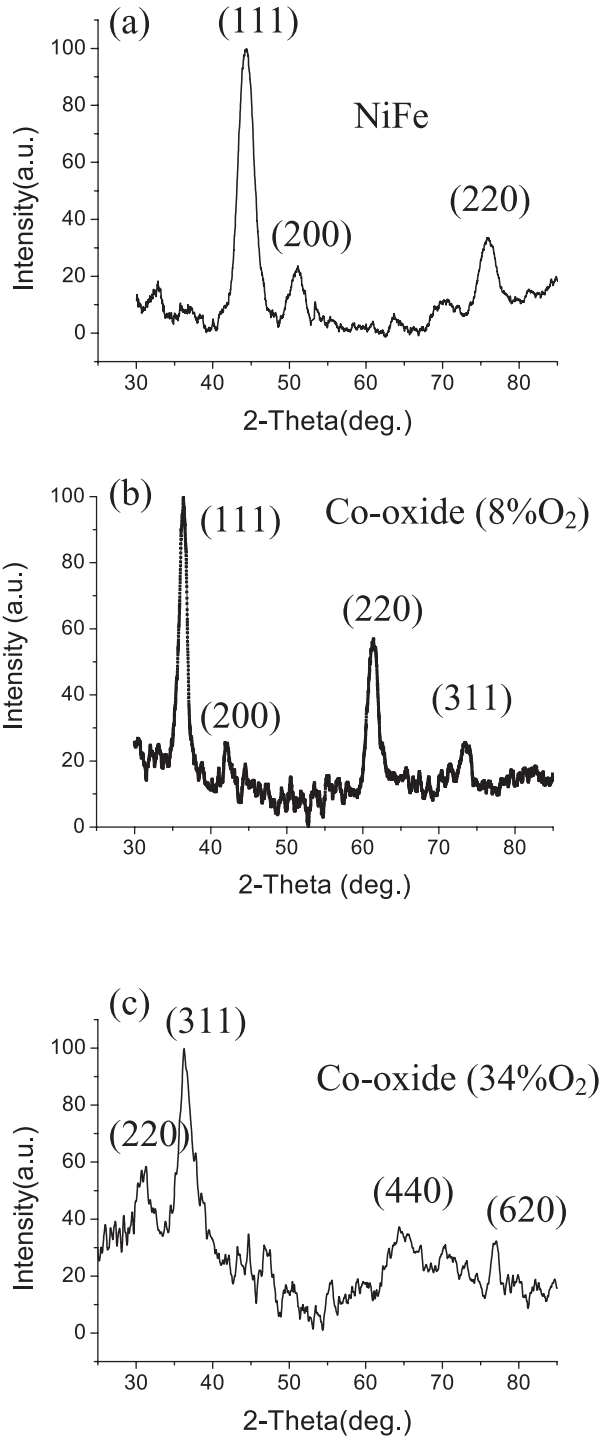

Fig. 1. Grazing angle X-ray diffraction patterns of (a) NiFe, (b) Co-oxide (8% O_2), and (c) Co-oxide (34% O_2) films.

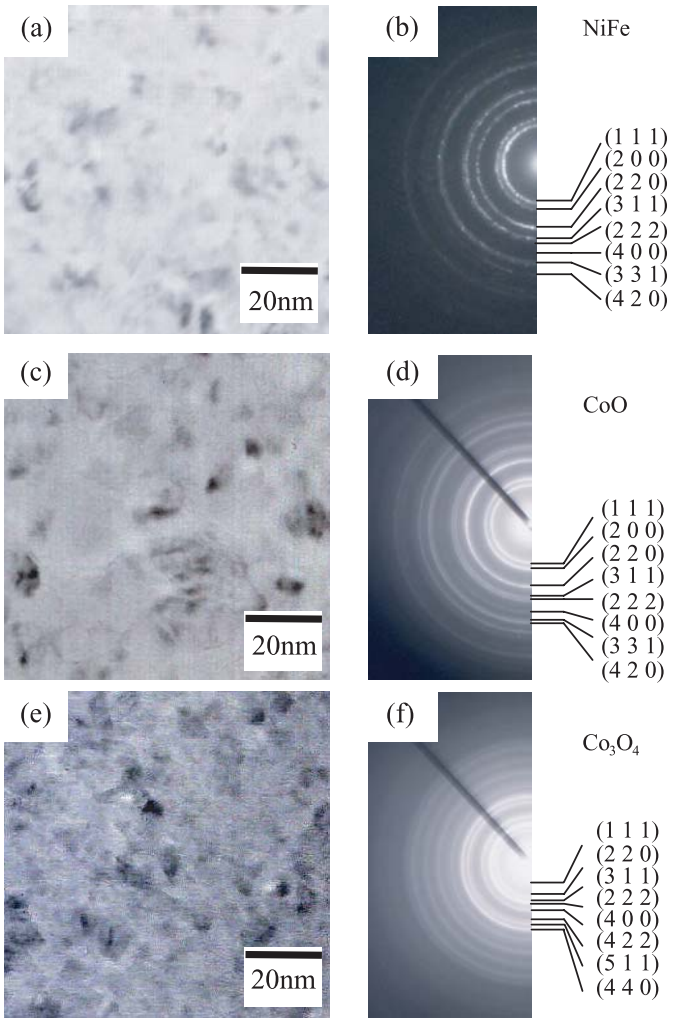

Fig. 2. Plan view TEM images of (a) $Ni_{80}Fe_{20}$, (c) Co-oxide (8% O_2), and (e) Co-oxide (34% O_2). Figures 2b, d, and f correspond to selected electron diffraction patterns.

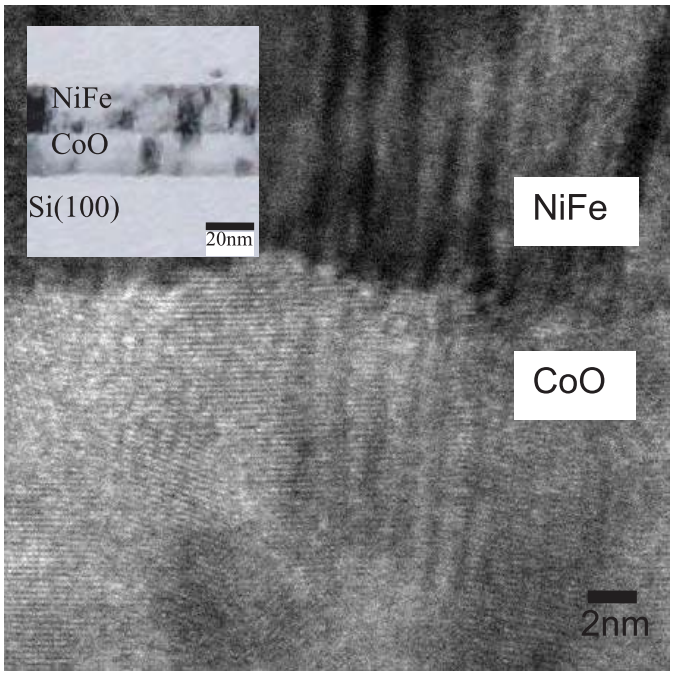

Fig. 3. Cross-sectional TEM micrograph of a $Ni_{80}Fe_{20}$/CoO bilayer grown on a Si(100) substrate.

distinguished in the electron diffraction patterns shown in Figure 2d and Figure 2f, respectively. Thus the possibility that films prepared with 34% O_2 in the assist beam consist of a mixture of CoO and Co_3O_4 can be excluded. Hecq et al. [17] have reported the mechanism of cobalt oxide formation, and found that the forms of sputtered films (Co, CoO and Co_3O_4) depend on the oxygen partial pressure. Qualitatively, our results in different forms of Co-oxides are in good agreement with the above mentioned mechanism for films prepared by this dual ion-beam deposition technique. The lattice constants of CoO and Co_3O_4 prepared by ion-beam sputtering are slight larger than those of bulk values, possibly due to the energetic oxygen incorporated into the lattice of CoO and Co_3O_4, respectively. Furthermore, the grain sizes of these $Ni_{80}Fe_{20}$ and Co-oxides, as estimated from both bright-field and dark-field images, range from 3 nm to 10 nm, which is significantly smaller than the film thickness (∼20 nm).

The cross-sectional TEM (Fig. 3) micrograph clearly shows that each polycrystalline layer exhibits a columnar structure perpendicular to the film surface and no obvious interdiffusion is present between the $Ni_{80}Fe_{20}$ and CoO interface. The lattice spacing of the CoO layer can be seen clearly and has been determined to be $d_{(111)} = 2.49$ Å.

The magnetic hysteresis loops of single NiFe layer, NiFe/Co bilayers, and $Ni_{80}Fe_{20}$/Co-oxide bilayers measured at $T = 289$ K are shown in Figure 4. The pure Permalloy layer deposited on Si(100) substrates exhibits the expected soft magnetic property of $H_c \sim 1$ Oe with an in-plane easy magnetization as a result of the shape (Fig. 4a). The saturation magnetization $M_s \sim 720$ emu/cm^3 is smaller than the bulk value of $Ni_{80}Fe_{20}$ (800 emu/cm^3) [24]. The NiFe/Co bilayer exhibits a higher coercivity of ∼10 Oe. This can be attributed to direct coupling between the magnetically hard Co and the magnetically soft NiFe layer that creates this room temperature magnetic behavior of the whole film. As can be seen in Figure 4b, the NiFe/Co bilayer switches in one step. The small saturation field ($H_{sat} \sim 50$ Oe) of NiFe/Co bilayers indicates that the easy axis lies in the film plane from shape anisotropy. On the other hand, $Ni_{80}Fe_{20}$/CoO bilayer (Fig. 4c) exhibits an enhanced coercivity, $H_c \sim 25$ Oe, compared to $Ni_{80}Fe_{20}$/Co bilayers (Fig. 4b) or $Ni_{80}Fe_{20}/Co_3O_4$ bilayers (Fig. 4d). This implies that the magnetic behavior of $Ni_{80}Fe_{20}$ layers drastically changes when it is covered by different forms of Co-oxides (CoO or Co_3O_4).

The coercivities and exchange fields of these $Ni_{80}Fe_{20}$/Co-oxide bilayers as a function of oxygen percentage in the assist beam measured at $T = 289$ K is shown in Figure 5. The zero exchange bias field is expected as there is no magnetic field applied during deposition. The NiFe/Co bilayers exhibit a coercivity of

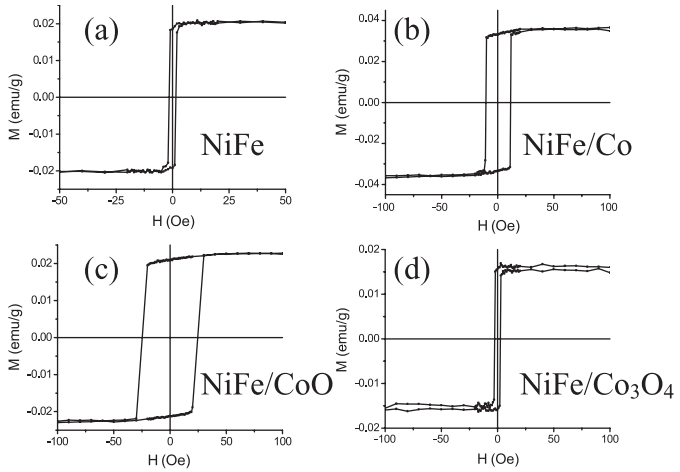

Fig. 4. Magnetic hysteresis loops at $T = 289$ K for (a) a pure NiFe layer, (b) NiFe/Co bilayer, (c) NiFe/Co-oxide (8% O_2) bilayer, and (d) NiFe/Co-oxide (34% O_2) bilayer.

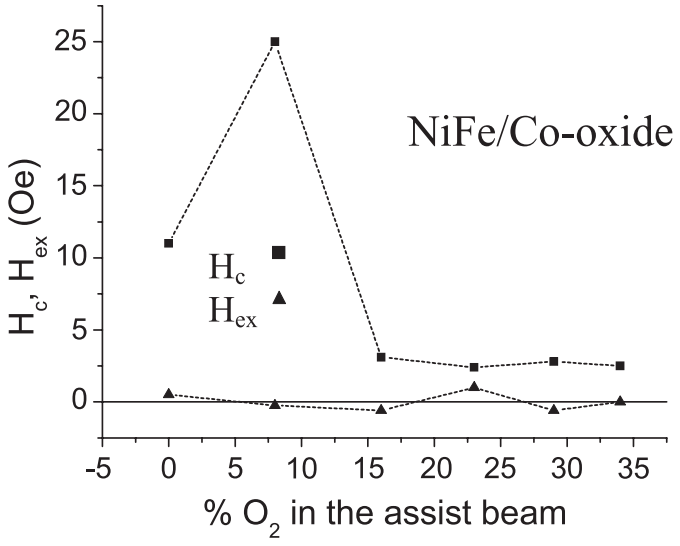

Fig. 5. The coercivities and exchange bias fields of NiFe/Co-oxide bilayers measured at $T = 289$ K.

$H_c \sim 10$ Oe, compared to the reference pure Permalloy layer ($H_c \sim 1$ Oe). The enhanced coercivity ($H_c \sim 25$ Oe) for films prepared with 8% O_2 in the assist beam indicates the existence of exchange coupling between $Ni_{80}Fe_{20}$ and CoO phases. The small coercivities ($H_c \sim 2$ Oe) for films prepared from 15% O_2 to 34% O_2 imply that structures of Co-oxide in these compositional ranges consist of mainly Co_3O_4, consistent with results obtained by TEM. Since the Néel temperature of bulk Co_3O_4 is $T_N \sim 30$ K [25], there is no exchange coupling between the paramagnetic Co_3O_4 (from 15% O_2 to 34% O_2 in the assist beam) and ferromagnetic $Ni_{80}Fe_{20}$ at the temperature of these measurements, and only the magnetic properties of the $Ni_{80}Fe_{20}$ layer are measured.

To examine the exchange interactions in the NiFe/Co-oxide bilayers, measurements of the temperature dependence of H_{ex} and H_c were carried out. The NiFe/Co-oxide (8% O_2) bilayer exhibits a significant shift in the hysteresis

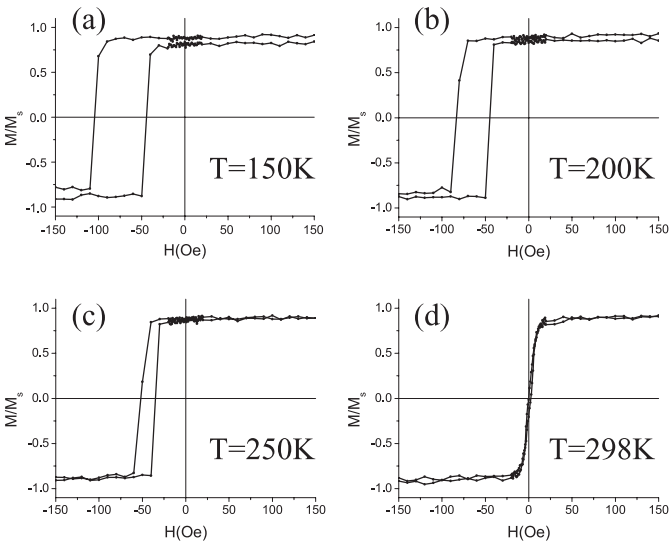

Fig. 6. Magnetic hysteresis loops of the NiFe/Co-oxide (8%O_2) bilayers measured at (a) 150 K, (b) 200 K, (c) 250 K, and (d) 298 K.

loop at 150 K, as shown in Figure 6a. This sample shows a strong temperature increase in $H_{ex} \sim -75$ Oe with cooling to 150 K that decreases with increasing temperature (Fig. 6b and c) and vanishes at 298 K, as shown in Figure 6d. This clearly shows the exchange coupling between ferromagnetic NiFe and antiferromagnetic CoO at temperatures below the Néel temperature of CoO ($T_N \sim 293$ K).

In order to gain insight into the origin of the coercivity and exchange bias, the NiFe thickness dependences for the coercivity and exchange field at 200 K and 298 K are shown in Figure 7. It is known [3,4] that both the coercivity and exchange bias vary as $H \propto 1/t_F^n$, where t_F is the thickness of the ferromagnetic layer and the exponent n (=1$\sim$ 2) is dependent on grain size and thickness for the ferromagnetic layer [5,26,27]. The coercivity and exchange field of NiFe/Co-oxide (8% O_2) bilayers at $T = 200$ K increases with decreasing NiFe thickness. However, both H_c and H_{ex} of NiFe/Co-oxide bilayers at $T = 298$ K (the vicinity of $T_{N\mathrm{CoO}}$) becomes almost thickness independent as shown in Figure 7. This clearly demonstrates that the exchange coupling interaction disappears at temperatures above the transition temperature (T_N) of CoO. Similar results in Fe/MnF_2 system have been reported by Leighton et al. [28].

The temperature dependence of coercivity H_c and exchange field H_{ex} of two $Ni_{80}Fe_{20}$/Co-oxide bilayers (8% and 34%) is shown in Figure 8. The hysteresis loops were measured parallel to the film surface after being field-cooled (FC) down to 10 K in a 20 kOe. Warming from T= 10 K, the coercivity ($H_c \sim 170$ Oe) decreases linearly with increasing temperature for films prepared with 34% O_2 in the assist beam. Additionally, an exchange shift $H_{ex} \sim -200$ Oe persists to temperatures greater than 30 K (the Néel temperature of bulk Co_3O_4). On the other hand, films prepared with 8% O_2 in the assist beam show an exchange field of $H_{ex} \sim -125$ Oe at $T = 10$ K,

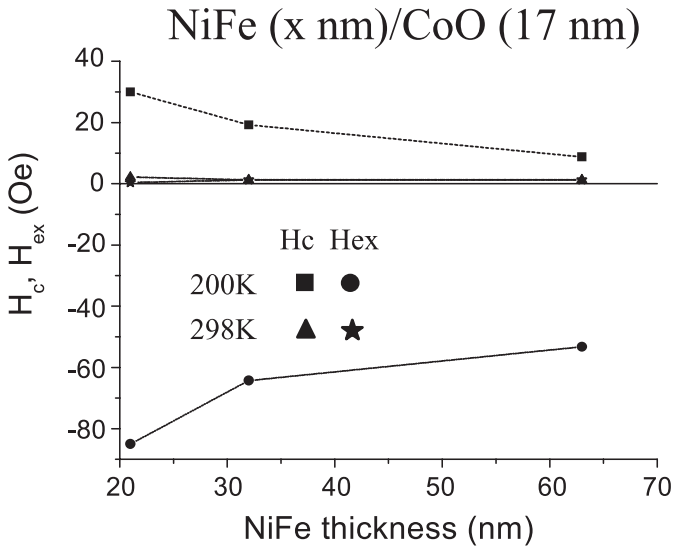

Fig. 7. NiFe thickness dependence of coercivities H_c and exchange fields H_{ex} of NiFe/Co-oxide (8% O_2) bilayers at 200 K and 298 K.

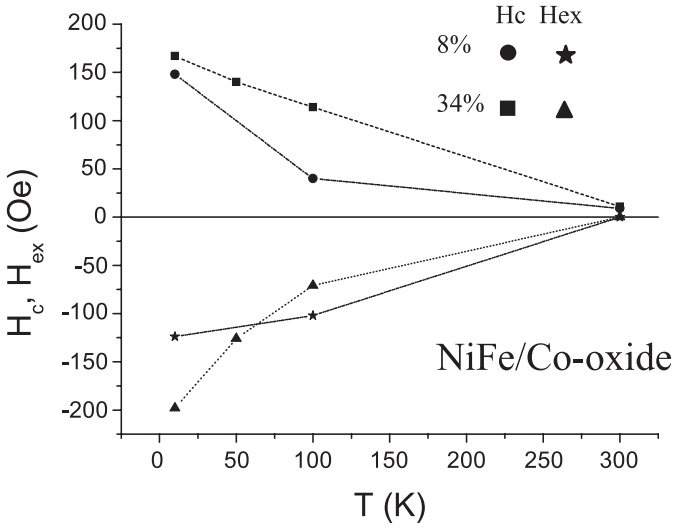

Fig. 8. Temperature dependence of H_c and H_{ex} of NiFe (21 nm)/Co-oxides (17 nm) (8% and 34% O_2) bilayers.

smaller than that for films prepared with 34% O_2 in the assist beam. In addition, the corresponding coercivities drop quickly, compared to those for films prepared with 34% O_2 in the assist beam. The lower limit of interfacial energy [7] ($H_{ex} \times M_s \times t_{d\,\mathrm{FM}}$) has been determined to be $E_{int} \sim 0.3$ erg/cm^2 (34% O_2) and ~0.19 erg/cm^2 (8% O_2) at $T = 10$ K. The different values in interfacial energy may be related to AF stiffness [18,19], direct coupling between AF and FM atoms [29], or interface disorder [6]. The larger exchange field (or interfacial energy) at $T = 10$ K for higher oxygen contents indicates the Co_3O_4 phase exhibits a stronger exchange coupling to $Ni_{80}Fe_{20}$, compared to that in $Ni_{80}Fe_{20}$/CoO bilayer, which is especially dominant below the Néel temperature of bulk Co_3O_4 ($T_N \sim 30$ K). This is surprising considering the significantly lower magnetocrystalline anisotropy of Co_3O_4 compared to CoO.

To clarify the relationship between the ferromagnetic domain formation and exchange bias in the NiFe/Co-oxide bilayers, AFM/MFM measurements were performed at $T = 289$ K, shown in Figure 9. The AFM image of NiFe/Co bilayer (Fig. 9a) shows a continuous NiFe layer with a root mean square (rms) roughness of 0.3 nm, similar to that of NiFe/CoO bilayer (Fig. 9c). Furthermore, the pure NiFe/Co bilayer exhibits ripple domains (Fig. 9b) whereas cross-tie domain walls (Fig. 9d) appear in the NiFe/CoO bilayer, as revealed by MFM images. Exchange bias, explained by competition between interfacial energy and anisotropy energy [30], depends on the density of cross-tie domains [20]. Recently Liu and Adenwalla [20] have reported that when the AF layer thickness is less than the critical thickness (~15 nm), enhanced coercivity but no loop shifting was observed, attributed to a small anisotropy energy of the AF layer (characterized by $K_{\mathrm{AF}}t_{\mathrm{AF}}$). Similar results have been observed in our NiFe (21 nm)/CoO (17 nm) bilayers. It should be noted

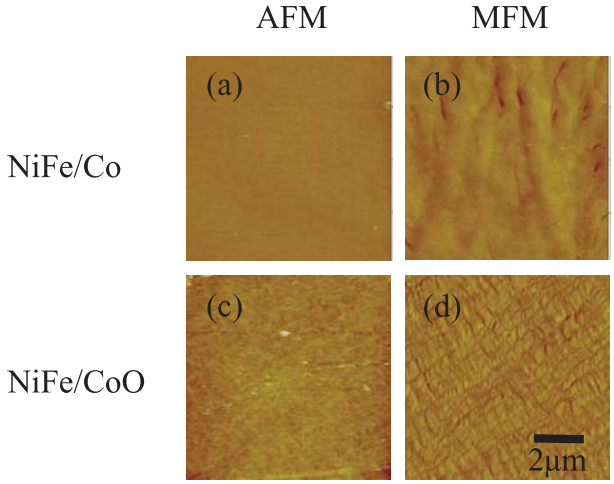

Fig. 9. AFM and MFM images of NiFe/Co bilayers (9a, b) and NiFe/Co-oxide (8% O_2) bilayers (9c, d) measured at $T = 289$ K.

that the grains of Co-oxides (8% and 34%) seem to be of the same size and these Co-oxide layers exhibit the same roughness, as revealed by TEM micrographs and AFM sectional analysis, respectively. However, the observed domain structures (ripple or cross-tie domains) are quite different, depending on the magnetic structure of the underlayer (Co or CoO). Therefore, these results obtained by microstructural and magnetic characterization lead us to conclude that the measured enhanced coercivity but zero exchange field of NiFe/CoO bilayers is attributed to the small anisotropy energy. The onset of an exchange bias field and a cross-tie domain structure would be expected if one were increase the antiferromagnetic CoO thickness.

4 Conclusions

Polycrystalline $Ni_{80}Fe_{20}$/Co-oxide bilayers have been successfully fabricated by a dual ion-beam deposition technique. The structure of the Co-oxide layer was varied from rock-salt CoO to spinel Co_3O_4 by controlling the O_2/Ar ratio from the assist source. A strong temperature dependence of the coercivity H_c and exchange bias field H_{ex} was found in these $Ni_{80}Fe_{20}$/Co-oxide bilayers. At $T = 10$ K, the $Ni_{80}Fe_{20}/Co_3O_4$ bilayer exhibited an exchange bias loop shift $H_{ex} \sim -200$ Oe, which was larger than that of the $Ni_{80}Fe_{20}$/CoO bilayer ($H_{ex} \sim -125$ Oe). The larger exchange field of $Ni_{80}Fe_{20}/Co_3O_4$ bilayer over $Ni_{80}Fe_{20}$/CoO bilayer at $T = 10$ K indicates the important role of the Co_3O_4 phase in exchange coupling to the $Ni_{80}Fe_{20}$ layer, and is especially dominant below the Néel temperature of bulk Co_3O_4. Surprisingly, there is evidence of exchange coupling above the bulk Néel temperature of Co_3O_4. This is a strong indication that the FM/AFM transition temperature in this film system has been raised by exchange coupling to the permalloy layer. A more detailed physical and theoretical analysis is currently underway to understand this unusual behavior. We tentatively attribute this magnetic behavior to the ferromagnetic NiFe altering the magnetic ordering of the Co_3O_4 underlayer during the cooling process. The enhanced coercivity of NiFe/CoO bilayers, compared to that of NiFe/Co bilayers, may be due to the exchange coupling between ferromagnetic NiFe and antiferromagnetic CoO, as revealed by a change in magnetic structures from ripple domains to cross-tie domains.

K.-W. Lin thanks Dr. J. van Lierop of the University of Manitoba, Canada for stimulating discussion and careful proofreading. The authors acknowledged help from K.-J. Lin, M.-D. Lan, J.-L. Tsai, and S.-A. Chen. This work was supported in part by the National Science Council of Taiwan under Grant No. NSC-92-2216-E-005-022.

References

1. W.H. Miklejohn, C.P. Bean, Phys. Rev. **102**, 1413 (1956)
2. V. Skumryev, S. Stoyanov, Y. Zhang, G. Hadjipanayis, D. Givord, J. Nogues, Nature **423**, 850 (2003)
3. J. Nogues, I. K. Schuller, J. Magn. Magn. Mater. **192**, 203 (1999)
4. A.E. Berkowitz, K. Takano, J. Magn. Magn. Mater. **200**, 552 (1999)
5. M.D. Stiles, R.D. McMichael, Phys. Rev. B **63**, 064405 (2001)
6. M. Finazzi, Phys. Rev. B **69**, 064405 (2004)
7. M. Gruyters, D. Riegel, Phys. Rev. B **63**, 052401 (2000)
8. K.-W. Lin, R. J. Gambino, L.H. Lewis, J. Appl. Phys. **93**, 6590 (2003)
9. K.-W. Lin, R.J. Gambino, L.H. Lewis, Jpn J. Appl. Phys. **44** (in press)
10. T.J. Regan, H. Ohldag, C. Stamm, F. Nolting, J. Luning, J. Stohr, R.L. White, Phys. Rev. B **64**, 214422 (2001)
11. J.S. Moodera, L.R. Kinder, J. Appl. Phys. **79**, 4724 (1996)
12. M. Gruyters, D. Riegel, J. Appl. Phys. **88**, 6610 (2000)
13. C.-H. Lai, Y.-H. Wang, C.-R. Chang, J.-S. Yang, Y.-D. Yao, Phys. Rev. B **64**, 094420 (2001)
14. Y.J. Tang, D.J. Smith, B.L. Zink, F. Hellman, A.E. Berkowitz, Phys. Rev. B **67**, 054408 (2003)
15. I.N. Krivorotov, T. Gredig, K.R. Nikolaev, A.M. Goldman, E. Dan. Dahlberg, Phys. Rev. B **65**, 180406 (2002)
16. O. Kubaschewski, E.L. Evans, C.B. Alcock, *Metallurgical Thermochemistry* (Pergamon Press, 1979)
17. M. Hecq, A. Hecqet, J. Van Cakenberghe, Thin Solid Films **42**, 97 (1977)
18. D. Mauri, H.C. Siegmann, P.S. Bagus, E. Kay, J. Appl. Phys. **62**, 3047 (1987)
19. A.P. Malozemoff, J. Appl. Phys. **63**, 3874 (1988)
20. Z.Y. Liu, S. Adenwalla, Appl. Phys. Lett. **82**, 2106 (2003)
21. H. Matsuyama, C. Haginoya, K. Koike, Phys. Rev. Lett. **85**, 646 (2000)
22. K.-W. Lin, F.-T. Lin, Y.-M. Tzeng, Jpn J. Appl. Phys. **44** (in press)
23. K.-W. Lin, F.-T. Lin, Y.-M. Tzeng, IEEE Trans. Magn. **41**, 927 (2005)
24. R.C. O'Handley, *Modern Magnetic Materials* (Wiley, New York, 2000)
25. S.A. Makhlouf, J. Magn, Magn. Mater. **246**, 184 (2002)
26. D.V. Dimitrov, S. Zhang, J.Q. Xiao, G.C. Hadjipanayis, C. Prados, Phys. Rev. B **58**, 2090 (1998)
27. S. Zhang, D.V. Dimitrov, G.C. Hadjipanayis, J.W. Cai, C.L. Chien, J. Magn. Magn. Mater. **198-199**, 468 (1999)
28. C. Leighton, M.R. Fitzsimmons, A. Hoffmann, J. Dura, C.F. Majkrzak, M.S. Lund, Ivan. K. Shculler, Phys. Rev. B **65**, 064403 (2002)
29. K. Takano et al., Phys. Rev. Lett. **79**, 1130 (1997)
30. B. Beschoten, P. Miltenyi, J. Keller, G. Guntherodt, J. Magn. Magn. Mater. **240**, 248 (2002)